Analyst

ROYAL SOCIETY OF CHEMISTRY

PAPER

View Article Online
View Journal | View Issue



Cite this: *Analyst*, 2023, **148**, 5619

# A photoluminescent and electrochemiluminescent probe based on an iridium(III) complex with a boronic acid-functionalised ancillary ligand for the selective detection of mercury(II) ions†

Kyoung-Rok Kim, Jinrok Oh and Jong-In Hong *

Exposure to mercury(II) ions ($Hg^{2+}$) can cause various diseases such as Minamata disease, acrodynia, Alzheimer's disease, and Hunter–Russell syndrome, and even organ damage. Therefore, real-time and accurate monitoring of $Hg^{2+}$ in environmental samples is crucial. In this study, we report a photoluminescent (PL) and electrochemiluminescent (ECL) probe based on a cyclometalated Ir(III) complex for the selective detection of $Hg^{2+}$. The introduction of a reaction site, *o*-aminomethylphenylboronic acid, on the ancillary ligands allowed a prompt transmetalation reaction to take place between $Hg^{2+}$ and boronic acid. This reaction resulted in significant decreases of the PL and ECL signals due to the photo-induced electron transfer from the Ir(III) complex to the $Hg^{2+}$ ions. The probe was applied to the selective detection of $Hg^{2+}$, and the signal changes revealed a linear correlation with $Hg^{2+}$ concentrations in the range of 0–10 μM (LOD = 0.72 μM for PL, 8.03 nM for ECL). The designed probe allowed the successful quantification of $Hg^{2+}$ in tap water samples, which proves its potential for the selective detection of $Hg^{2+}$ in environmental samples.

Received 25th July 2023,
Accepted 1st October 2023

DOI: 10.1039/d3an01266b

rsc.li/analyst



## Introduction

Rapid industrialisation has resulted in the frequent release of toxic chemicals, which can cause serious environmental problems. Among various released chemicals, the mercury(II) ion ($Hg^{2+}$) is classified as a persistent, bio-accumulative, and toxic chemical, and is considered a threat to humans and the environment.[1] Although $Hg^{2+}$ is colourless, tasteless, and odourless, it can be easily absorbed into the body through the cell membranes of the skin, respiratory tract, and gastrointestinal tract.[2] The assimilation of $Hg^{2+}$ in the human body can damage the central nervous system, endocrine glands, and organs.[3,4] Furthermore, chronic exposure to $Hg^{2+}$ has been associated with various diseases, such as Minamata disease, acrodynia, Alzheimer's disease, and Hunter–Russell syndrome.[5] Consequently, the U.S. Environmental Protection Agency (EPA) has recommended that the maximum level of inorganic mercury in drinking water is 10 nM.[6] The common methods employed for the detection of $Hg^{2+}$ include inductively coupled plasma atomic emission spectroscopy (ICP-AES),[7] atomic absorption spectroscopy,[8,9] electrochemical analysis,[10–12] surface-enhanced Raman spectroscopy (SERS),[13,14] piezoelectric detection,[15] and colourimetric and fluorometric detection.[16] In particular, fluorescent chemosensors for $Hg^{2+}$ have been developed based on the $Hg^{2+}$-catalysed reaction and coordination of heteroatoms with $Hg^{2+}$.[17] However, these detection methods are very expensive and time-consuming, and require skilled laboratory professionals. Furthermore, they require bulky and fragile instrumental setup, including an additional optical source.

Electrochemiluminescence (ECL) is a luminescence process involving sequential electron transfers between electrogenerated species on an electrode surface.[18] Compared with the photoluminescence (PL) process, ECL offers several advantages due to its low background signal and high sensitivity. In addition, ECL rarely requires complicated procedures, complex conditions, or bulky equipment for analysis.[18–20] Consequently, ECL has been considered a powerful tool for real-time, on-site sample analysis, and several studies have reported systems that combine the ECL technique with chemosensors.[21–41] So far, most ECL molecular probes have been developed using tris(2,2′-bipyridine)ruthenium(II) complexes ($[Ru(bpy)_3^{2+}]$) with their characteristically low metal-centred state (MC state), making it challenging to adjust the wavelength with changes in the molecular structure.[42] Among various luminophores considered as replacements for Ru(II) complexes, Ir(III) complexes are regarded as promising ECL

*Department of Chemistry, Seoul National University, 1 Gwanak-ro, Gwanak-gu, Seoul 151-747, Korea. E-mail: jihong@snu.ac.kr*

† Electronic supplementary information (ESI) available. See DOI: https://doi.org/10.1039/d3an01266b

luminophores due to their high ECL quantum yields and colour tunability through ligand modification by high ligand field stabilization energies.[33,43–48] Hong and co-workers reported the first ECL analysis system for the detection of $Hg^{2+}$ ions based on the reaction of a small molecular probe with these ions.[35] Unfortunately, this system could not be applied in field monitoring because large amounts of organic solvents were required. Consequently, the development of new ECL probes with high selectivity and sensitivity toward $Hg^{2+}$ in aqueous solutions is greatly desired.

Herein, we report a new PL and ECL chemodosimetric probe based on an iridium(III) complex for the determination of $Hg^{2+}$ (Scheme 1). The design strategy of probe **1** is based on the following: (i) $[Ir(piq)_2(bpy)][PF_6]$ (piq = 1-phenylisoquinoline, bpy = bipyridine) was selected as a luminophore, and (ii) *o*-aminomethylphenylboronic acid was introduced into the ancillary ligand as a PL and ECL signalling modulator, as well as a reaction site for the $Hg^{2+}$ ions.[49–53] Probe **1** was expected to exhibit significant PL and ECL changes towards $Hg^{2+}$ ions in aqueous solutions when compared to other Ir(III)-based probes because this probe has cationic charge and hydrophilic *o*-aminomethylphenylboronic acid, which imparts high solubility in aqueous solutions. Probe **1** promptly reacted with $Hg^{2+}$ ions through the transmetalation reaction to generate **1**-$Hg^{2+}$, resulting in decreased PL and ECL signals. Probe **1**, as analysed through PL and ECL, exhibited high sensitivity and selectivity in detecting $Hg^{2+}$ ions within 2 min in aqueous solutions with small amounts of organic solvent (10% acetonitrile). These results imply significant potential for on-site $Hg^{2+}$ detection, compared with other PL-based chemodosimeters, as illustrated in Table S1.† In addition, probe **1** was successfully applied to ECL analysis of $Hg^{2+}$ ions in tap water samples.

## Experimental

Probes **1** and **2** were synthesised as shown in Scheme 2. Detailed synthetic procedures for compounds **1–11** are provided in the ESI.†

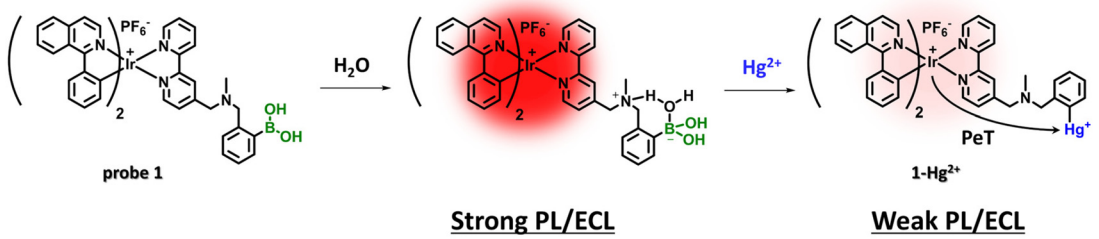


**Scheme 1** The detection mechanism of probe **1** for $Hg^{2+}$ ions.

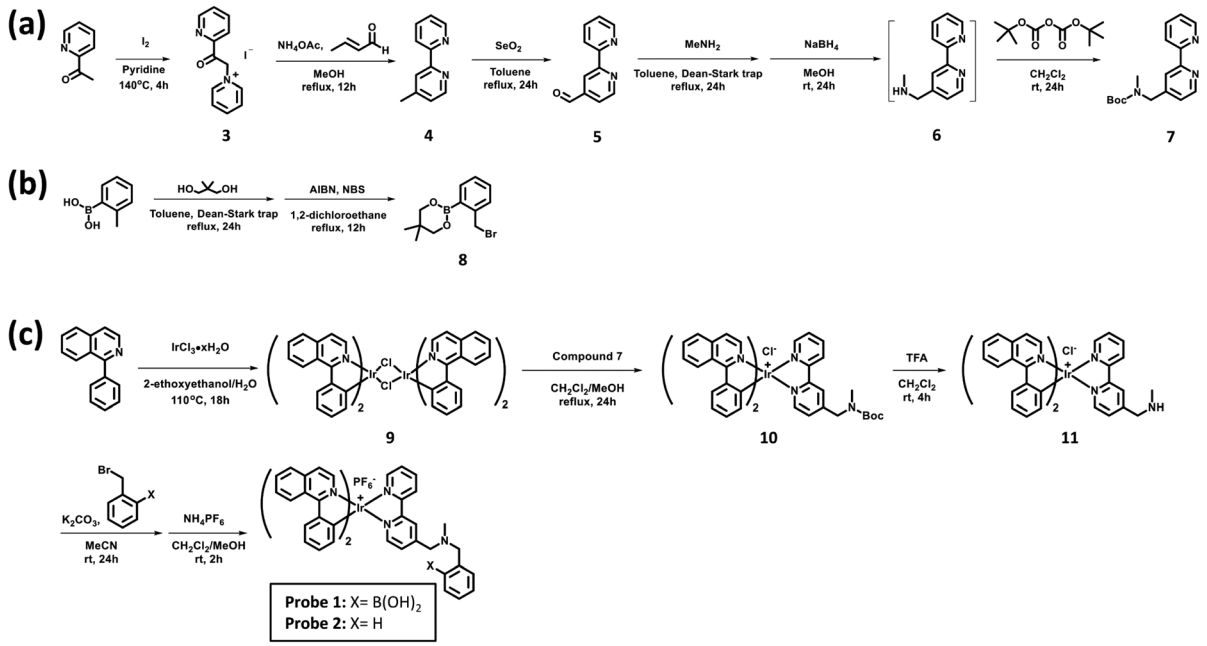


**Scheme 2** Synthetic routes of (a) compound **7**, (b) compound **8**, and (c) probes **1** and **2**.

### Synthesis of 1

A mixture of crude compound **11** (17 mg, 20 μmol), compound **8** (7 mg, 25 μmol), and potassium carbonate (13 mg, 94 μmol) in 0.2 mL of acetonitrile was stirred at room temperature for 12 h. The solvent was evaporated under reduced pressure and extracted with dichloromethane three times. The organic phase was washed with water and brine, dried over anhydrous sodium sulphate, and evaporated. The residue was purified by silica gel column chromatography (acetonitrile/$H_2O$/sat. $KNO_3$(aq) = 40 : 4 : 1). The product was re-dissolved in dichloromethane/methanol (1 : 1, 1 mL) and stirred at room temperature for 2 h with potassium hexafluorophosphate (37 mg, 0.2 mmol). The solution was filtered, and the filtrate was evaporated under reduced pressure. The residue was triturated with dichloromethane and diethylether. The resulting precipitate was filtered, washed with diethylether and dried *in vacuo* to afford **1** (10 mg, 47%). $^1$H NMR (300 MHz, $CDCl_3$) $\delta$ 8.99–8.84 (m, 2H), 8.78 (d, $J$ = 8.2 Hz, 1H), 8.60 (s, 1H), 8.44 (s, 2H), 8.28–8.20 (m, 2H), 8.10 (t, $J$ = 7.3 Hz, 1H), 7.89 (dd, $J$ = 6.2, 3.0 Hz, 2H), 7.80–7.69 (m, 6H), 7.64 (d, $J$ = 5.6 Hz, 1H), 7.40–7.28 (m, 8H), 7.22 (d, $J$ = 7.1 Hz, 1H), 7.10 (t, $J$ = 7.6 Hz, 2H), 6.88 (t, $J$ = 7.0 Hz, 2H), 6.25 (d, $J$ = 7.3 Hz, 2H), 3.82 (d, $J$ = 5.5 Hz, 4H), 2.28 (s, 3H). $^{13}$C NMR (126 MHz, $CD_3CN$) $\delta$ 168.49, 168.45, 156.01, 155.25, 153.47, 153.38, 150.68, 150.61, 145.57, 145.53, 140.80, 140.68, 139.47, 137.09, 137.07, 135.92, 131.98, 131.87, 130.86, 130.83, 130.75, 130.57, 130.50, 129.14, 129.02, 129.01, 128.64, 128.48, 127.56, 127.54, 127.45, 126.76, 126.75, 126.17, 126.15, 125.63, 124.86, 122.32, 122.30, 121.98, 121.90, 62.75, 58.55, 40.79. LRMS (MALDI-TOF) $m/z$: $[M]^+$ calc. for $C_{49}H_{40}BIrN_5O_2$ 934.290, found 934.063. HRMS (FAB) $m/z$: $[M - H_2O]^+$ calc. for $C_{49}H_{38}BIrN_5O$ 916.2799, found 916.2793.

### Synthesis of 2

A mixture of crude compound **11** (9 mg, 11 μmol), benzyl bromide (4 mg, 23 μmol), potassium iodide (4 mg, 24 μmol), and potassium carbonate (3 mg, 22 μmol) in 0.2 mL of acetonitrile was stirred at room temperature for 12 h. The solvent was evaporated under reduced pressure and extracted with dichloromethane three times. The organic phase was washed with water and brine, dried over anhydrous sodium sulphate, and evaporated. The residue was re-dissolved in dichloromethane/methanol (1 : 1, 1 mL) and stirred at room temperature for 2 h with ammonium hexafluorophosphate (18 mg, 0.11 mmol). The solution was filtered and evaporated, and the residue was purified by silica gel column chromatography ($CH_2Cl_2$/MeOH = 50 : 1) to afford **2** (6 mg, 53%). $^1$H NMR (400 MHz, $CDCl_3$) $\delta$ 8.92 (dd, $J$ = 5.9, 3.1 Hz, 2H), 8.73 (d, $J$ = 8.2 Hz, 1H), 8.58 (s, 1H), 8.26 (d, $J$ = 8.0 Hz, 2H), 8.15 (t, $J$ = 7.8 Hz, 1H), 7.90 (dd, $J$ = 6.3, 3.1 Hz, 2H), 7.77 (dd, $J$ = 6.4, 3.2 Hz, 4H), 7.72 (d, $J$ = 4.9 Hz, 1H), 7.63 (d, $J$ = 5.4 Hz, 1H), 7.49 (d, $J$ = 20.2 Hz, 1H), 7.36 (m, $J$ = 6.5 Hz, 7H), 7.28 (d, $J$ = 7.3 Hz, 2H), 7.20 (d, $J$ = 6.8 Hz, 1H), 7.11 (t, $J$ = 7.6 Hz, 2H), 6.89 (t, $J$ = 7.4 Hz, 2H), 6.27 (t, $J$ = 6.6 Hz, 2H), 3.70 (d, $J$ = 72.2 Hz, 4H), 2.26 (s, 3H). $^{13}$C NMR (125 MHz, $CDCl_3$) $\delta$ 169.04, 168.99, 155.65, 155.47, 153.55, 153.41, 150.11, 145.47, 145.41, 140.21, 139.71, 136.99, 132.17, 131.70, 130.87, 130.85, 130.68, 130.66, 128.70, 128.49, 127.99, 127.59, 127.57, 126.93, 126.88, 126.31, 126.26, 125.38, 122.29, 121.98, 121.96, 62.03, 29.68. HRMS (FAB) $m/z$: $[M]^+$ calc. for $C_{49}H_{39}IrN_5$ 890.2835, found 890.2834.

## Results and discussion

### Spectroscopic properties of 1

We checked the changes in the UV-vis and PL spectra of probe **1** in the presence and absence of $Hg^{2+}$ in an aqueous medium (pH 7.4, HEPES buffer/$CH_3CN$ = 9 : 1, v/v). Probe **1** displayed an intense absorption peak at 288 nm, which was attributed to the spin-allowed ligand-centred ($^1$LC) transition states (Fig. S1†). Furthermore, the broad absorption peak detected around 330–510 nm was attributed to the mixing of metal-to-ligand charge-transfer ($^1$MLCT and $^3$MLCT) transitions, ligand-centred ($^3$LC) transitions, and ligand-to-ligand charge-transfer ($^3$LLCT and $^1$LLCT) transitions.[54] When the concentration of $Hg^{2+}$ ions in solution increased, the absorption bands of probe **1** showed a slight red-shift. Subsequently, the PL response of probe **1** to $Hg^{2+}$ was evaluated. As the amount of $Hg^{2+}$ increased, the PL signal ($\lambda_{ex}$ = 400 nm) gradually decreased until it reached a plateau after the addition of 10 μM $Hg^{2+}$ (Fig. 1a). This indicated that probe **1** reacted in 1 : 1 stoichio-

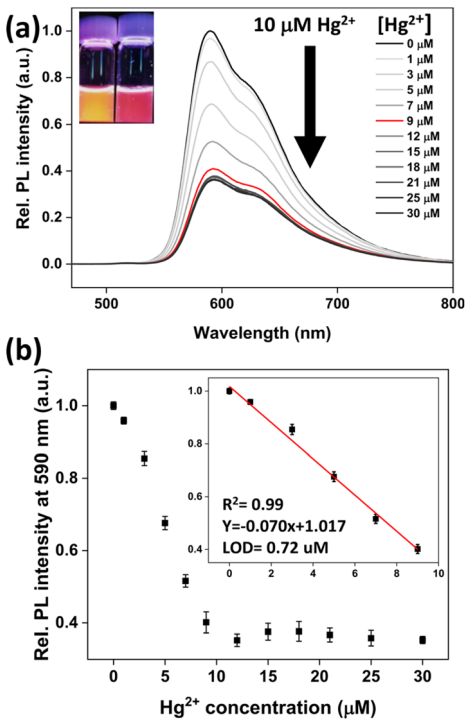


**Fig. 1** (a) PL emission spectra ($\lambda_{ex}$ = 400 nm) of probe **1** (10 μM) with increasing $Hg^{2+}$ ion concentrations in $CH_3CN/H_2O$ (1 : 9 v/v, pH 7.4, 10 mM HEPES). Inset: photographs of the probe solutions without and with $Hg^{2+}$ under 365 nm UV irradiation. (b) PL intensity changes of probe **1** at 590 nm upon the addition of $Hg^{2+}$ ions. Inset: a linear correlation between the PL intensity at 590 nm and the concentration of $Hg^{2+}$.

metry with $Hg^{2+}$. The limit of detection (LOD) was 0.73 μM from the linear correlation ($R^2$ = 0.99) between the concentration of $Hg^{2+}$ ions (in the range of 0–10 μM) and the PL intensity (Fig. 1b).

To further understand the quenching behaviour of probe **1** in the presence of $Hg^{2+}$, its fluorescence lifetimes before and after the addition of $Hg^{2+}$ ions were measured by time-correlated single-photon counting, whereby this probe exhibited single-exponential decay with a lifetime of 0.82 μs (Fig. S2a†). However, in the presence of $Hg^{2+}$ ions, an additional shorter lifetime of ~0.1 μs was observed, thus revealing double-exponential decay in the PL decay curve. This can be attributed to the generation of the reaction product, **1**-$Hg^{2+}$, *via* the transmetalation reaction between $Hg^{2+}$ and boronic acid on the ancillary ligands. Upon the addition of $Hg^{2+}$, the lifetimes decreased, thus indicating that the quenching mechanism was highly dependent on dynamic quenching (Fig. S2b†).[55–57] These changes were observed with the addition of up to 10 μM $Hg^{2+}$ ions, which were consistent with the signal change trends observed in the PL response experiments.

To determine the selectivity of probe **1** in an aqueous solution, the PL spectra were measured in the presence of various metal ions. As expected, the PL of probe **1** decreased effectively only in the presence of $Hg^{2+}$, whereas other metal ions exhibited negligible PL signal changes (Fig. 2). This selectivity can be attributed to the transmetalation between phenylboronic acid and $Hg^{2+}$ ions.[49–53] The PL of **1**-$Hg^{2+}$ generated through the reaction between probe **1** and $Hg^{2+}$ was quenched by the electron transfer from the excited Ir(III) complex to $Hg^{2+}$.[58]

To investigate the probe's pH susceptibility, the PL intensity of probe **1** was measured in the pH range of 4–10 after the addition of $Hg^{2+}$ (Fig. 3a). The probe showed a significant change in PL in the presence of $Hg^{2+}$ over a wide pH range of 5–9, thus confirming its high stability in the detection of $Hg^{2+}$. The relatively weaker $Hg^{2+}$ responses observed at pH 4 and 10 were presumably due to inefficient formation of boronate and generation of mercury(II) hydroxide, respectively.[59,60] Subsequently, the sensing ability toward $Hg^{2+}$ ions in different ratios of $CH_3CN$–HEPES buffer solution was evaluated (Fig. 3b). Upon increasing the ratio of the HEPES buffer solution in the $CH_3CN$–HEPES buffer solution, a remarkable PL signal change in the presence of $Hg^{2+}$ was observed since in an aqueous solution *o*-aminomethylphenylboronic acid undergoes $H_2O$ insertion to generate boronate.[60] Since the formation of boronate is essential in a transmetalation reaction,[61–63] the reaction of probe **1** with $Hg^{2+}$ ions occurred more efficiently in solutions with high $H_2O$ content. Therefore, a significant PL response of probe **1** toward $Hg^{2+}$ was induced in a 1 : 9 $CH_3CN$–HEPES buffer solution. The PL intensity of probe **1** was saturated within 2 minutes in the presence of 10 μM $Hg^{2+}$ ions, indicating that $Hg^{2+}$ ions could be detected quickly under our experimental conditions (Fig. S3†).

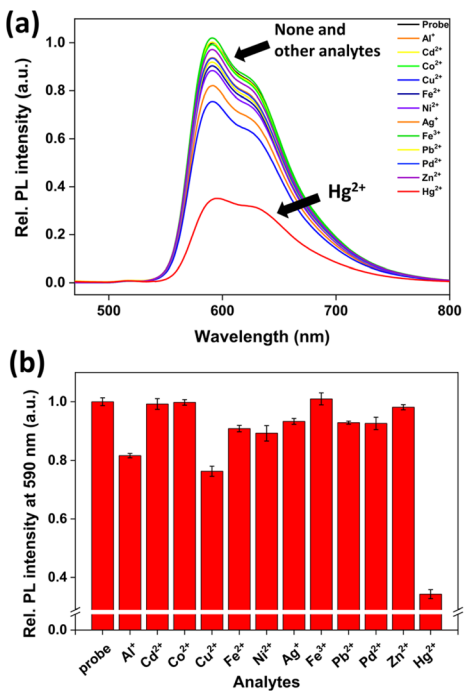


**Fig. 2** (a) PL emission spectra ($\lambda_{ex}$ = 400 nm) of probe **1** (10 μM) in the presence of various analytes (40 μM each; $Hg^{2+}$, 20 μM) in $CH_3CN/H_2O$ (1 : 9 v/v, pH 7.4, 10 mM HEPES). (b) PL emission intensities at 590 nm of probe **1** (10 μM) upon the respective addition of various metal ions (40 μM).

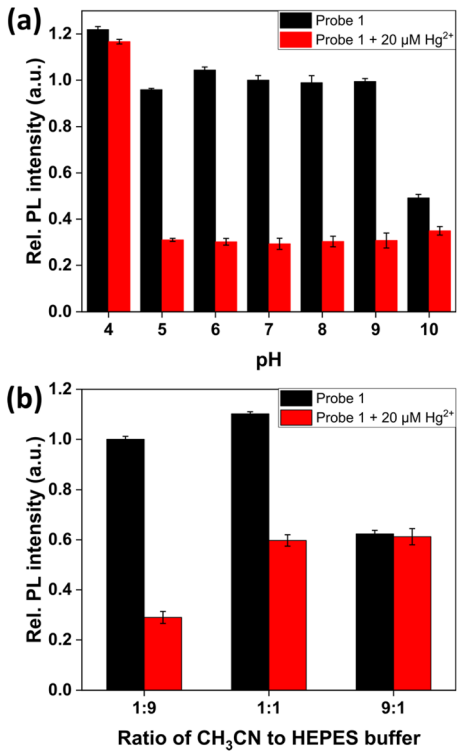


**Fig. 3** PL intensity changes of probe **1** (10 μM, $\lambda_{em}$ = 590 nm, $\lambda_{ex}$ = 400 nm) towards 20 μM $Hg^{2+}$ ions (a) in $CH_3CN/H_2O$ (1 : 9 v/v, pH 7.4, 10 mM HEPES) under varying pH conditions and (b) in different ratios of $CH_3CN$ to 10 mM HEPES buffer solution (pH = 7.40).

### Proposed sensing mechanism

$^1$H nuclear magnetic resonance (NMR) experiments with probe **1** in $CD_3CN/D_2O$ (1 : 1) were then conducted (Fig. S4†). Upon the addition of $Hg^{2+}$ ions to probe **1**, the signals at 3.75 ppm corresponding to the two methylene protons connected to the tertiary nitrogen were slightly downfield-shifted because of the binding of $Hg^{2+}$ and the tertiary amine. However, after the addition of an excess amount of $Hg^{2+}$ ions, the proton signals significantly decreased, and two new methylene proton peaks appeared at 3.72 and 3.53 ppm due to the reaction between boronic acid and $Hg^{2+}$ ions. Similarly, the methyl proton signal at 2.25 ppm moved gradually downfield with the addition of $Hg^{2+}$ ions with a decreased intensity, while a new peak appeared at 2.21 ppm with an increased intensity. High-performance liquid chromatography coupled with Thermo Scientific linear ion trap-orbitrap mass spectrometry (HPLC-LTQ-orbitrap) analysis was performed to confirm the reaction product generated after the addition of $Hg^{2+}$ ions (Fig. S5†). Before the addition of $Hg^{2+}$ ions, an *m*/*z* signal appeared at 934.6, which was attributed to probe **1**. Upon the addition of 20 μM $Hg^{2+}$ ions to probe **1**, the *m*/*z* signal of probe **1** disappeared, and a major peak at 1115.6 appeared, which was attributed to **1**-$Hg^{2+}$. Both NMR and HPLC-LTQ-orbitrap analyses confirmed that probe **1** reacted effectively with $Hg^{2+}$ through transmetalation to generate **1**-$Hg^{2+}$.

To confirm the role of boronic acid in the PL and ECL signal changes with $Hg^{2+}$ ions, probe **2** without boronic acid was designed. The PL of probe **1** significantly decreased in the presence of 20 μM $Hg^{2+}$ ions, while probe **2** hardly showed any PL changes, even after the addition of an excess amount of $Hg^{2+}$ ions (Fig. 4). These results indicated that the transmetalation of boronic acid with $Hg^{2+}$ ions is essential in the PL/ECL sensing mechanism.

To verify the signal changes in PL, an electrochemical analysis with DPV was performed (Fig. S6 and Table S2†). The highest occupied molecular orbital (HOMO) and lowest unoccupied molecular orbital (LUMO) energy levels of probe **1** were calculated to be −5.78 and −3.12 eV, respectively. Meanwhile, a mixture of probe **1** and 10 μM $Hg^{2+}$ ions revealed a new peak at −0.54 V (*vs.* $Fc/Fc^+$), which was attributed to the LUMO energy level (−4.26 eV) of –$Hg^+$, while the HOMO and LUMO energy levels of the Ir(III) complex were similar to those of probe **1**. The LUMO energy level of –$Hg^+$ lies between the HOMO and LUMO levels of the Ir(III) complex (Fig. S7†), which indicated that the PL signals of probe **1** were restrained by the photo-induced electron transfer (PeT) process from the Ir(III) complex to –$Hg^+$. Therefore, probe **1** showed decreased PL signals in the presence of $Hg^{2+}$. Meanwhile, **1**-$Hg^{2+}$ showed a more stabilised LUMO energy level by 0.13 eV compared to probe **1** due to the mercury cation introduced into probe **1** through the transmetalation reaction. These results are in accordance with the red-shift tendency observed in the UV-vis absorption spectra of probe **1** with $Hg^{2+}$ ions (Fig. S1†).

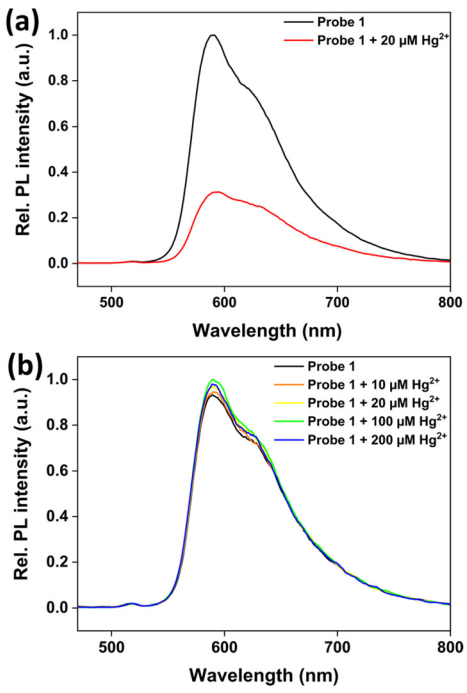


**Fig. 4** PL intensity changes of (a) probe **1** and (b) probe **2** (10 μM) upon the addition of $Hg^{2+}$ ions in $CH_3CN/H_2O$ (1 : 9 v/v, pH 7.4, 10 mM HEPES).

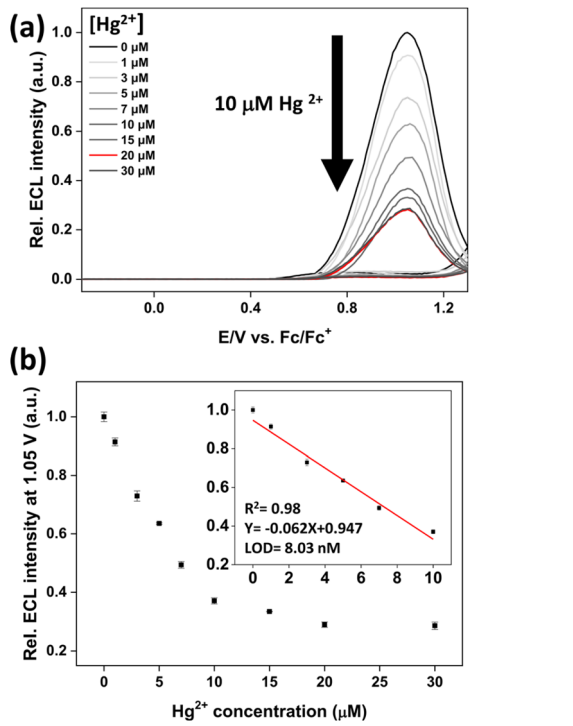


**Fig. 5** (a) ECL intensities of probe **1** (10 μM) upon the addition of $Hg^{2+}$ in $CH_3CN/H_2O$ (1 : 9 v/v, pH 7.4, 100 mM DBAE, 0.1 M HEPES, 0.1% polidocanol and 0.1 M TBAP as the supporting electrolyte) while the potential is swept at a GC disk electrode (diameter 2 mm) in the range of −0.3–1.3 V (scan rate: 0.1 V $s^{-1}$). (b) ECL intensity changes of probe **1** at 1.05 V upon the addition of $Hg^{2+}$. Inset: a linear correlation between the ECL intensity at 1.05 V and the concentration of $Hg^{2+}$.

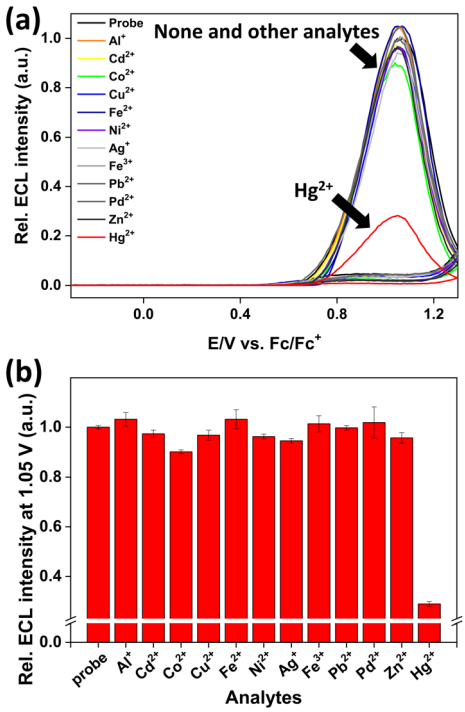


**Fig. 6** (a) ECL intensities of probe **1** (10 μM) in the presence of various metal ions (40 μM each; $Hg^{2+}$ 20 μM) in $CH_3CN/H_2O$ (1 : 9 v/v, pH 7.4, 100 mM DBAE, 0.1 M HEPES, 0.1% polidocanol, and 0.1 M TBAP as the supporting electrolyte) while the potential is swept at a GC disk electrode (diameter 2 mm) in the range of −0.3–1.3 V (scan rate: 0.1 V $s^{-1}$). (b) ECL intensities at 1.05 V of probe **1** (10 μM) upon the respective addition of various metal ions (40 μM) and $Hg^{2+}$ ions (20 μM).

### ECL properties of 1

Fig. 5a shows the ECL emission profile during cyclic voltammetry in aqueous media (pH 7.4, HEPES buffer/$CH_3CN$ = 9 : 1 v/v, 0.1 M 2-(dibutylamino)ethanol (DBAE), 0.1 M HEPES, 0.1% polidocanol, and 0.1 M tetrabutylammonium perchlorate (TBAP) as the supporting electrolyte). Probe **1** produced a strong ECL signal around 1.05 V. However, the ECL signals gradually decreased as the amounts of $Hg^{2+}$ increased. Interestingly, the ECL signals showed a linear correlation with $Hg^{2+}$ concentrations in the range of 0–10 μM (Fig. 5b, $R^2$ = 0.98) with a LOD of 8.03 nM, which was much lower than the LOD determined by the PL method. This value falls below the maximum allowable contaminant level of mercury in drinking water recommended by the U.S. EPA. The high sensitivity of probe **1** demonstrates its ability to effectively detect $Hg^{2+}$ ions in waste streams, which can have significant adverse effects on the environment.

As shown in Fig. 6, the ECL intensity of probe **1** did not show any significant changes upon the addition of other metal ions; however, a significant decrease in the ECL signal (~20% that of probe **1**) was observed after the addition of 20 μM (2 equiv.) of $Hg^{2+}$. The designed system showed rapid reaction rate, high sensitivity, and remarkable selectivity toward $Hg^{2+}$ ions, thus offering a new practical method for field monitoring of $Hg^{2+}$ ions.

Consequently, probe **1** can be used as a highly selective $Hg^{2+}$ probe based on ECL analysis (Scheme 3). Probe **1** was directly oxidised on glassy carbon (GC) electrodes to form $\mathbf{1}^{\bullet+}$. Subsequently, it was turned into the excited state, 1*, by one-electron transfer from the DBAE radical (DBAE$^{\bullet}$), which emitted red ECL. In the presence of $Hg^{2+}$, probe **1** rapidly reacted with $Hg^{2+}$ *via* an irreversible transmetalation reaction to generate **1**-$Hg^{2+}$. The excited state of **1**-$Hg^{2+}$ was formed *via* a mechanism similar to that of probe **1** when oxidation occurs on the GC electrode. However, (**1**-$Hg^{2+}$)* was rapidly consumed through an immediate PeT process from (**1**-$Hg^{2+}$)* to –$Hg^{+}$, resulting in a significant decrease in the ECL intensity (Fig. S7†).

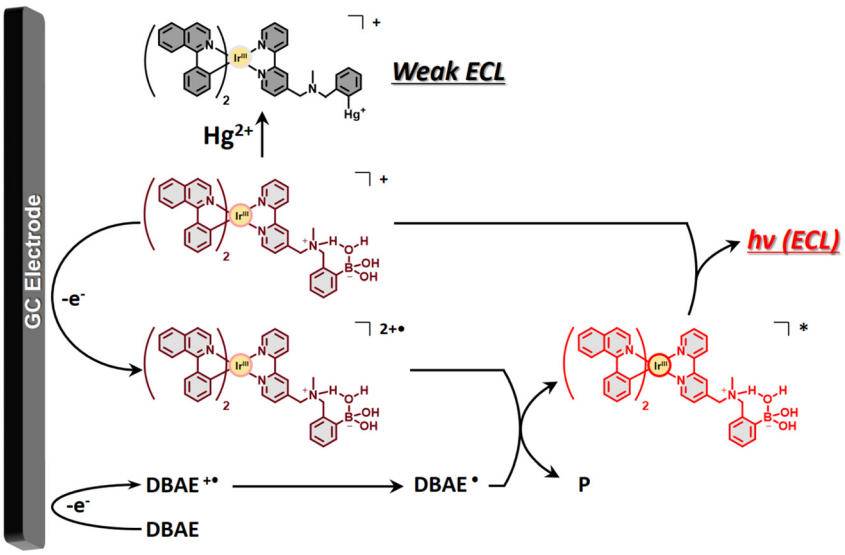


**Scheme 3** The proposed sensing mechanism of probe **1** for detection of $Hg^{2+}$ ions through ECL analysis.

Table 1 Quantification of $Hg^{2+}$ in tap water samples[a]

| $[Hg^{2+}]_{added}$ [b] | Rel. ECL intensity (experiment, $n = 3$) | $[Hg^{2+}]_{calc'd}$ (μM) | Recovery (%) |
|---|---|---|---|
| 0 μM | 1 ± 0.0167 | — | — |
| 3 μM | 0.7514 ± 0.0028 | 3.1780 ± 0.0347 | 105.93 ± 1.10 |
| 5 μM | 0.6371 ± 0.0071 | 5.0356 ± 0.1145 | 100.71 ± 2.27 |
| 7 μM | 0.5277 ± 0.0040 | 6.8137 ± 0.0655 | 97.34 ± 0.96 |
| 10 μM | 0.3409 ± 0.0068 | 9.8500 ± 0.1107 | 98.50 ± 1.12 |

[a] All ECL intensities were measured along with the cyclic voltammetry (CV) scan in $CH_3CN/H_2O$ (1 : 9 v/v, pH 7.4, 100 mM DBAE, 0.1 M HEPES, 0.1% polidocanol, and 0.1 M TBAP) while the potential was swept at a GC working electrode in the range of −0.3–1.3 V *vs.* $Fc/Fc^+$. [b] Concentrations of $Hg^{2+}$ ions in tap water samples.

### Quantification of $Hg^{2+}$ ions in tap water

To confirm the reliability of the ECL sensing system in real samples, probe **1** was used to quantify $Hg^{2+}$ ions in tap water using the standard addition method. Analytical solutions were prepared by diluting 1 mL of tap water containing varying concentrations of $Hg^{2+}$ ions with 1 mL of $CH_3CN/H_2O$ (1 : 4 v/v, pH 7.4, 20 μM probe **1**, 200 mM DBAE, 0.2 M HEPES, 0.2% polidocanol, and 0.2 M TBAP). $Hg^{2+}$ ions in the diluted analytical solutions were quantified by comparing ECL values with the calibration curve shown in Fig. 5b. Then, the actual concentrations of $Hg^{2+}$ ions in tap water samples were accurately determined by multiplying the values obtained from the calibration curve by the dilution factor of 2. First, the ECL emission of probe **1** in tap water was assessed and almost no change in the ECL signal occurred prior to the addition of $Hg^{2+}$ (Table 1). This observation was made in comparison with the ECL intensity of probe **1** in $CH_3CN/H_2O$ (as shown in the inset of Fig. 5b), suggesting that the tap water sample contained a negligible amount of $Hg^{2+}$. As the concentration of $Hg^{2+}$ ions increased, the ECL signal of probe **1** decreased. The recovery rates for $Hg^{2+}$ ions ranged from 97.34% to 105.93%, indicating the high reliability and feasibility of this system for the detection of $Hg^{2+}$ in actual environmental samples.

## Conclusions

In summary, we developed a novel photoluminescent (PL) and electrochemiluminescent (ECL) dual signalling probe based on an Ir(III) complex with boronic acid as the reaction site for the selective detection of $Hg^{2+}$ ions. PL and ECL analyses with the probe showed it had remarkable selectivity for $Hg^{2+}$ ions with limits of detection of 0.72 μM and 8.03 nM, respectively. Furthermore, the successful quantification of $Hg^{2+}$ ions in tap water samples using the ECL analysis demonstrated the effectiveness of this probe. Consequently, our system serves as a new proof-of-concept for real-time and on-site sample analysis. We believe that our strategy would be of great help to the advancement of developing ECL-based probes and other fields concerning ECL-based analysis.

## Conflicts of interest

There are no conflicts to declare.

## Acknowledgements

This work was supported by the NRF grant funded by the Korean Government (MSIT) (No. 2023R1A2C2006049).

## References

1 C. Kumunda, A. S. Adekunle, B. B. Mamba, N. W. Hlongwa and T. T. I. Nkambule, *Front. Mater.*, 2021, **7**, 616787.
2 B.-J. Ye, B.-G. Kim, M.-J. Jeon, S.-Y. Kim, H.-C. Kim, T.-W. Jang, H.-J. Chae, W.-J. Choi, M.-N. Ha and Y.-S. Hong, *Ann. Occup. Environ. Med.*, 2016, **28**, 5–5.
3 J. Mutter, J. Naumann, C. Sadaghiani, R. Schneider and H. Walach, *Neuroendocrinol. Lett.*, 2004, **25**, 331–339.
4 M. V. Yigit, A. Mishra, R. Tong, J. Cheng, G. C. L. Wong and Y. Lu, *Chem. Biol.*, 2009, **16**, 937–942.
5 A. Anandababu, S. Anandan and M. Ashokkumar, *ChemistrySelect*, 2018, **3**, 4413–4420.
6 W.-L. Cui, Z.-H. Zhang, L. Wang, J. Qu and J.-Y. Wang, *Spectrochim. Acta, Part A*, 2022, **267**, 120516.
7 Z. Zhu, G. C. Y. Chan, S. J. Ray, X. Zhang and G. M. Hieftje, *Anal. Chem.*, 2008, **80**, 7043–7050.
8 H. Erxleben and J. Ruzicka, *Anal. Chem.*, 2005, **77**, 5124–5128.
9 S. Gil, I. Lavilla and C. Bendicho, *Anal. Chem.*, 2006, **78**, 6260–6264.
10 S. Gupta, R. Singh, M. D. Anoop, V. Kulshrestha, D. N. Srivastava, K. Ray, S. L. Kothari, K. Awasthi and M. Kumar, *Appl. Phys. A*, 2018, **124**, 737.
11 S.-J. Liu, H.-G. Nie, J.-H. Jiang, G.-L. Shen and R.-Q. Yu, *Anal. Chem.*, 2009, **81**, 5724–5730.
12 A. Moutcine and A. Chtaini, *Sens. Bio-Sens. Res.*, 2018, **17**, 30–35.
13 Y. Du, R. Liu, B. Liu, S. Wang, M.-Y. Han and Z. Zhang, *Anal. Chem.*, 2013, **85**, 3160–3165.
14 S. J. Lee and M. Moskovits, *Nano Lett.*, 2011, **11**, 145–150.
15 D. P. Ruys, J. F. Andrade and O. M. Guimarães, *Anal. Chim. Acta*, 2000, **404**, 95–100.
16 G. Chen, Z. Guo, G. Zeng and L. Tang, *Analyst*, 2015, **140**, 5400–5443.
17 H. Shuai, C. Xiang, L. Qian, F. Bin, L. Xiaohui, D. Jipeng, Z. Chang, L. Jiahui and Z. Wenbin, *Dyes Pigm.*, 2021, **187**, 109125.
18 M. M. Richter, *Chem. Rev.*, 2004, **104**, 3003–3036.
19 M. Hesari and Z. Ding, *J. Electrochem. Soc.*, 2015, **163**, H3116–H3131.
20 W. Miao, *Chem. Rev.*, 2008, **108**, 2506–2553.
21 M. Schmittel and H.-W. Lin, *Angew. Chem., Int. Ed.*, 2007, **46**, 893–896.

22 E. Berni, I. Gosse, D. Badocco, P. Pastore, N. Sojic and S. Pinet, *Chem. – Eur. J.*, 2009, **15**, 5145–5152.
23 W. Zhang, D. Zhao, R. Zhang, Z. Ye, G. Wang, J. Yuan and M. Yang, *Analyst*, 2011, **136**, 1867–1872.
24 J.-W. Oh, T. H. Kim, S. W. Yoo, Y. O. Lee, Y. Lee, H. Kim, J. Kim and J. S. Kim, *Sens. Actuators, B*, 2013, **177**, 813–817.
25 K. Chen and M. Schmittel, *Chem. Commun.*, 2014, **50**, 5756–5759.
26 P. Li, Z. Jin, M. Zhao, Y. Xu, Y. Guo and D. Xiao, *Dalton Trans.*, 2015, **44**, 2208–2216.
27 H. Li, A. C. Sedgwick, M. Li, R. A. R. Blackburn, S. D. Bull, S. Arbault, T. D. James and N. Sojic, *Chem. Commun.*, 2016, **52**, 12845–12848.
28 Y. Xu, L. Zhang, Y. Liu, Z. Jin, Q. Zhao, F. Yang and D. Xiao, *Biosens. Bioelectron.*, 2016, **77**, 182–187.
29 D. Han, M. Qian, H. Gao, B. Wang, H. Qi and C. Zhang, *Anal. Chim. Acta*, 2019, **1074**, 98–107.
30 F. Yuan, K. Hao, S. Sheng, T. H. Fereja, X. Ma, F. Liu, M. N. Zafar, B. Lou, H. Tian and G. Xu, *Electrochim. Acta*, 2020, **329**, 135117.
31 Y. Dai, Z. Zhan, L. Chai, L. Zhang, Q. Guo, K. Zhang and Y. Lv, *Anal. Chem.*, 2021, **93**, 4628–4634.
32 I.-S. Shin, S. W. Bae, H. Kim and J.-I. Hong, *Anal. Chem.*, 2010, **82**, 8259–8265.
33 H. J. Kim, K.-S. Lee, Y.-J. Jeon, I.-S. Shin and J.-I. Hong, *Biosens. Bioelectron.*, 2017, **91**, 497–503.
34 S.-Y. Kim, H. J. Kim and J.-I. Hong, *RSC Adv.*, 2017, **7**, 10865–10868.
35 H. Rhee, T. Kim and J.-I. Hong, *Dalton Trans.*, 2018, **47**, 3803–3810.
36 K.-R. Kim, H. J. Kim and J.-I. Hong, *Anal. Chem.*, 2019, **91**, 1353–1359.
37 T. Kim and J.-I. Hong, *ACS Omega*, 2019, **4**, 12616–12625.
38 J. Park, T. Kim, H. J. Kim and J.-I. Hong, *Dalton Trans.*, 2019, **48**, 4565–4573.
39 H. J. Kim, T. Kim and J.-I. Hong, *Sens. Actuators, B*, 2020, **307**, 127656.
40 T. Kim, H. J. Kim, I.-S. Shin and J.-I. Hong, *Anal. Chem.*, 2020, **92**, 6019–6025.
41 Y. Namkoong, J. Oh and J.-I. Hong, *Chem. Commun.*, 2020, **56**, 7577–7580.
42 H. Wei and E. Wang, *Luminescence*, 2011, **26**, 77–85.
43 J. M. Fernandez-Hernandez, E. Longhi, R. Cysewski, F. Polo, H.-P. Josel and L. De Cola, *Anal. Chem.*, 2016, **88**, 4174–4178.
44 E. Kerr, E. H. Doeven, D. J. D. Wilson, C. F. Hogan and P. S. Francis, *Analyst*, 2016, **141**, 62–69.
45 J. I. Kim, I.-S. Shin, H. Kim and J.-K. Lee, *J. Am. Chem. Soc.*, 2005, **127**, 1614–1615.
46 E. Longhi, J. M. Fernandez-Hernandez, A. Iordache, R. Fröhlich, H.-P. Josel and L. De Cola, *Inorg. Chem.*, 2020, **59**, 7435–7443.
47 Z. M. Smith, E. Kerr, E. H. Doeven, T. U. Connell, N. W. Barnett, P. S. Donnelly, S. J. Haswell and P. S. Francis, *Analyst*, 2016, **141**, 2140–2144.
48 Y. Zhou, K. Xie, R. Leng, L. Kong, C. Liu, Q. Zhang and X. Wang, *Dalton Trans.*, 2017, **46**, 355–363.
49 A. Chatterjee, M. Banerjee, D. G. Khandare, R. U. Gawas, S. C. Mascarenhas, A. Ganguly, R. Gupta and H. Joshi, *Anal. Chem.*, 2017, **89**, 12698–12704.
50 X. Guo, J. Huang, Y. Wei, Q. Zeng and L. Wang, *J. Hazard. Mater.*, 2020, **381**, 120969.
51 S. W. Lee, S. Y. Lee and S. H. Lee, *Tetrahedron Lett.*, 2019, **60**, 151048.
52 S. Subedi, L. N. Neupane, P. K. Mehta and K.-H. Lee, *Dyes Pigm.*, 2021, **191**, 109374.
53 S. Subedi, L. N. Neupane, H. Yu and K.-H. Lee, *Sens. Actuators, B*, 2021, **338**, 129814.
54 M. Lepeltier, B. Graff, J. Lalevée, G. Wantz, M. Ibrahim-Ouali, D. Gigmes and F. Dumur, *Org. Electron.*, 2016, **37**, 24–34.
55 J. R. Lakowicz, *Principles of fluorescence spectroscopy*, Springer, New York, 2006.
56 A. S. Tanwar, L. R. Adil, M. A. Afroz and P. K. Iyer, *ACS Sens.*, 2018, **3**, 1451–1461.
57 A. S. Tanwar, R. Parui, R. Garai, M. A. Chanu and P. K. Iyer, *ACS Meas. Sci. Au*, 2022, **2**, 23–30.
58 J. H. He, Y. Y. Cheng, T. Yang, H. Y. Zou and C. Z. Huang, *Anal. Chim. Acta*, 2018, **1035**, 203–210.
59 M. Tian, C. Wang, Q. Ma, Y. Bai, J. Sun and C. Ding, *ACS Omega*, 2020, **5**, 18176–18184.
60 X. Sun, B. M. Chapin, P. Metola, B. Collins, B. Wang, T. D. James and E. V. Anslyn, *Nat. Chem.*, 2019, **11**, 768–778.
61 A. J. J. Lennox and G. C. Lloyd-Jones, *Angew. Chem., Int. Ed.*, 2013, **52**, 7362–7370.
62 A. J. J. Lennox and G. C. Lloyd-Jones, *Chem. Soc. Rev.*, 2014, **43**, 412–443.
63 C. F. R. A. C. Lima, A. S. M. C. Rodrigues, V. L. M. Silva, A. M. S. Silva and L. M. N. B. F. Santos, *ChemCatChem*, 2014, **6**, 1291–1302.